JOURNAL OF GUIDANCE, CONTROL, AND DYNAMICS
Vol. 31, No. 6, November–December 2008

Determination of Spherical Test Mass Kinematics with Modular Gravitational Reference Sensor

John W. Conklin,* Graham Allen,† Ke-Xun Sun,‡ and Daniel B. DeBra§
Stanford University, Stanford, California 94305

DOI: 10.2514/1.34230

A modular gravitational reference sensor is stand-alone sensor for gravitational wave detection, inertial navigation, and fundamental physics experiments in space. In a modular design, measurement of the mass center of a drag-free test mass is made with respect to reference surfaces fixed to the spacecraft. In a gravitational wave detection scheme, the same reference surfaces are used to independently measure the distance between sensors on separate spacecraft. A single spinning spherical test mass is used as the gravitational reference, with several interferometers used to measure the mass center location relative to the spacecraft housing. This paper develops an analytical model for the modular gravitational reference sensor output including all first-order contributions. With this model, we evaluate systematic errors in the mass center measurement due to geometric variations which place requirements on spacecraft attitude and test mass dynamics. We also present a fast and reliable algorithm for recovering the mass center location and spin frequency of the test mass, in real time, to the required level of accuracy from the sensor data.

Nomenclature

A_{lm} = coefficient in spherical harmonic expansion of the test mass shape [see Eq. (5)]
c_{lm} = spherical harmonics normalization constant [see Eq. (7)]
H_n^k = complex amplitude of the nth harmonic of the precession frequency ω_p (or spin frequency ω_s) measured by sensor k [see Eqs. (12) and (21)]
h^k = distance from geometric center of housing to sensor k
$\mathbf{L}$ = test mass angular momentum vector
$\mathbf{p}$ = vector from mass center of test mass to geometric center of the housing
r_0 = nominal radius of the test mass [see Eq. (5)]
$\mathbf{s}^k$ = vector from the geometric center of the housing to sensor k
z^k = sensor k output [distance measurement, see Eq. (8)]
η^k = azimuthal angle to sensor k in the inertial frame
θ_p = polhode angle
ξ^k = polar angle to sensor k in the inertial frame
ϕ_p = polhode phase
ϕ_s = test mass spin phase $= -(\phi_p + \psi_p)$ when $\theta_p = 0$
ψ_p = precession phase
Ω_p = polhoder rate $= \dot{\phi}_p$
ω_p = precession rate $= \dot{\psi}_p$
$\boldsymbol{\omega}_s$ = test mass angular velocity vector

Superscript

k = sensor number

I. Introduction

THE Laser Interferometer Space Antenna (LISA) [1–3] and the Big Bang Observer (BBO) [4,5] are two proposed gravitational wave observatories requiring unprecedented precision in the measurement of the variations in the distance between the mass centers of test masses housed in drag-free spacecraft. A drag-free spacecraft contains and shields a test mass (TM) from external disturbances and, through the use of a feedback control system, follows the free-floating TM in a purely gravitational orbit [6]. At the heart of these missions is a gravitational reference sensor (GRS) which measures the test-mass mass center (MC) location for both the science measurement and the spacecraft drag-free control system.

The modular gravitational reference sensor (MGRS) [5,7,8], shown schematically in Fig. 1, is a candidate sensor for gravitational wave detection, as well as inertial navigation and fundamental physics experiments in space. The MGRS must provide two layers of precision for the measurement of the MC location of the test mass. For the science measurement, the MGRS must provide the MC location to 10 $\mathrm{pm}/\sqrt{\mathrm{Hz}}$ in the 0.1 mHz–1 Hz science frequency band, which is consistent with the science requirements for LISA [2]. The MGRS must also provide the MC location to 3 nm for the drag-free control system, which is required to maintain the spacecraft position to 30 nm with respect to the TM [2]. It is important to note the drag-free measurement is more than two orders of magnitude less accurate than the requirement for the science measurement. The drag-free control system bandwidth is determined by the disturbances to the spacecraft which is unrelated to the science data. For LISA, spacecraft disturbances are dominated by solar radiation pressure which occurs at frequencies much lower than 1 Hz. Therefore, depending on the application, the drag-free control bandwidth may be different than that of the science frequency band. This paper will mainly focus on the requirements for the science measurement, which is more challenging with respect to measurement of the MC location.

The MGRS uses a single spinning spherical test mass as the gravitational reference, with 12–18 optical displacement sensors used to measure the TM mass center location in three dimensions relative to the MGRS housing. The sphere is intentionally spun so that detection of the surface implies the location of the mass center. By spinning faster than the highest frequency of interest, say ∼10 Hz, the MC offset from the geometric center and the residual surface nonsphericity are shifted above the science frequency band so that they do not interfere with the MC location measurement. For BBO, where the science frequency band is 0.1–10 Hz, the spin frequency would be ∼100 Hz. However, because the value of the

---

Received 10 November 2007; revision received 2 February 2008; accepted for publication 5 February 2008.

*Doctoral Candidate, Department of Aeronautics & Astronautics, Durand Building, 496 Lomita Mall. AIAA Student Member.

†Doctoral Candidate, Department of Applied Physics, Stanford University, Via Pueblo Mall, Room 101.

‡Senior Research Scientist, Edward L. Ginzton Laboratory.

§Edward C. Wells Professor, Emeritus, Department of Aeronautics & Astronautics, 277 Durand, MC 4035. AIAA Fellow.

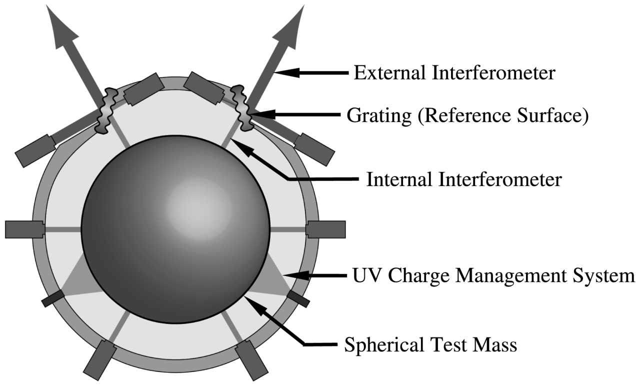

Fig. 1 Schematic of the MGRS design.

spin speed does not alter the analysis, we will only focus on the LISA frequency band for simplicity.

Except for residual geometric irregularities, the sphere is orientation invariant. Consequently, with a spherical TM, we can eliminate electrostatic suspension for TM orientation control, which can cause unwanted forcing of the TM. Once the requirement for orientation control is eliminated, a large gap (∼20 mm) between the housing and the TM surface can be used, which is the single most important design parameter with respect to disturbances. These three primary design features (a modular design, a single spherical TM, and a large gap) make the MGRS a simple and reliable sensor that meets the precision requirements for the next generation GRS.

In this paper, we review the dynamics of a torque-free rigid body, including polhode behavior, which serves as an accurate model for the TM motion. With the TM inertia tensor, the motion is parametrized and, with a plausible model for the TM geometry, a model for the output of each MGRS internal sensor is developed. This model includes all contributions above the sensor design noise limit of 3 $\mathrm{pm}/\sqrt{\mathrm{Hz}}$. With this model, potential systematic errors caused by geometric variations are evaluated, and limits are placed on the amplitude of spacecraft attitude variations in the science frequency band, the TM polhode decay rate, and spacecraft angular rates. Finally, we present a computationally tractable and robust algorithm for determining the TM MC location to the required level of 10 $\mathrm{pm}/\sqrt{\mathrm{Hz}}$ in the 0.1 mHz–1 Hz frequency band, as well as the TM spin frequency to better than a part in 10^6.

II. Polhode Motion

The dynamics of a spinning drag-free test mass can be accurately modeled by Euler's equations for the torque-free motion of a rigid body. Any such spinning body will undergo polhode motion, which is the motion of the instantaneous angular velocity vector $\boldsymbol{\omega}_s$ in the body [9]. The curve produced by $\boldsymbol{\omega}_s$ on the inertia ellipsoid is the *polhode*. In addition, $\boldsymbol{\omega}_s$ moves relative to the angular momentum vector $\mathbf{L}$ which is fixed in inertial space. We refer to this motion as the *precession* of the angular velocity vector.

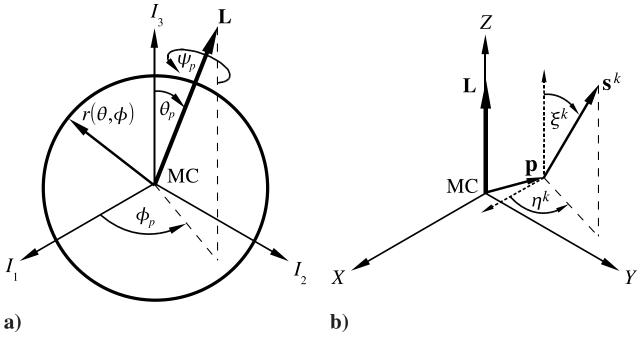

Fig. 2 Reference frames: a) body frame with I_1, I_2, I_3 axes where TM radius $r(\theta, \phi)$ is defined; b) inertial frame with X, Y, Z axes.

Even though the dynamics may seem quite complicated, we only require three Euler angles to fully describe the motion of the TM in an inertial frame. We first define a reference frame fixed to the TM, called the body frame, shown in Fig. 2a, with origin at the TM mass center and axes aligned with the I_1, I_2, and I_3 principal axes. Because no forces act on a drag-free TM, we can also use the MC as the origin of an inertial reference frame, with X, Y, Z coordinate axes, as shown in Fig. 2b. The Z axis is aligned with the TM angular momentum vector and the X and Y axes are made orthogonal. We choose a set of Euler angles ϕ_p, θ_p, and ψ_p, defined in Fig. 2a, to transform between these two frames. These angles are called the polhode phase, polhode angle, and precession phase. The relevance of these names will become apparent. The subscript p reminds us that these angles are related to the polhode motion of the TM. The following three successive rotations take us from the body frame to the inertial frame: 1) a positive rotation about the body I_3 axis by angle ϕ_p, 2) a positive rotation about the second axis (y axis) of the intermediate frame by angle θ_p to align I_3 with $\mathbf{L}$ (inertial Z), and 3) a positive rotation about the third axis (z axis) of the intermediate frame by angle ψ_p to produce the X, Y, Z inertial frame.

With this convention, we do not explicitly parametrize the polhode (i.e., the motion of $\boldsymbol{\omega}_s$ in the body frame). This is because we are only interested in the orientation of the TM in the inertial frame, where we make our measurement, and $\boldsymbol{\omega}_s$ is not necessarily fixed in inertial space. However, when $I_1 \sim I_2 \sim I_3$, $\boldsymbol{\omega}_s$ is closely aligned with $\mathbf{L}$, and the Euler angles ϕ_p and θ_p describe the polhode.

Lagrange's method can be used to derive a set of differential equations that define the rigid body motion of the TM in the inertial frame. We use generalized coordinates ϕ_p, θ_p, and ψ_p, and take the kinetic energy and the angular momentum $\mathbf{L}$ to be constants of the motion. This approach is similar to one described in [10], which uses a different set of Euler angles.

There are two fundamental frequencies arising from the rigid body motion of the TM that enter our measurement. One is the frequency associated with the precession rate $\omega_p \equiv \dot{\psi}_p$, which is very nearly the spin rate ω_s when $I_1 \sim I_2 \sim I_3$, or when $\boldsymbol{\omega}_s$ is close to one of the principal axes in an arbitrary body. In general, $L/I_2 \leq \omega_p \leq L/I_1$. The other fundamental frequency is associated with the polhode rate $\Omega_p \equiv \dot{\phi}_p$.

The polhode rate Ω_p is proportional to the spin rate ω_s. The constant of proportionality is governed by the inertia ellipsoid and the kinetic energy of the spinning body. With the three principal moments of inertia $I_1 < I_2 < I_3$ we can define the moment of inertia difference ratios k_1, k_2, and k_3 as follows:

$$k_1 = \frac{I_3 - I_2}{I_1} \qquad k_2 = \frac{I_1 - I_3}{I_2}$$
$$k_3 = \frac{I_2 - I_1}{I_3} \quad \text{with} \quad k_1 + k_2 + k_3 + k_1 k_2 k_3 = 0 \tag{1}$$

We would like $\boldsymbol{\omega}_s$ to be aligned with the axis of maximum moment of inertia for which the kinetic energy is a minimum for a constant angular momentum. Assuming that $\boldsymbol{\omega}_s$ is closely aligned with the I_3 axis, the polhode rate is roughly

$$\Omega_p \sim k_1 \omega_s \tag{2}$$

The shape of the polhode is governed by the asymmetry of the body, which can be parametrized by the moment of inertia difference ratios. From Eq. (1), we see that there are only two independent moment of inertia difference ratios that define the polhode. Let us take k_1 and k_3 as the independent set.

In general, $k_1 \neq k_3 \neq 0$ and we say the body is asymmetric and the polhode is an ellipse. For a closed elliptical polhode, the polhode rate Ω_p and the precession rate ω_p are modulated about a nominal value at twice the nominal polhode frequency.

In the special case of a symmetric body where one of the moment of inertia difference ratios is zero, say $k_3 = 0$, the polhode is circular. We will focus our attention on this case because, in the next section, we will see that the proposed MGRS test mass can be modeled as a symmetric body. For a closed circular polhode, Ω_p and ω_p are constants that can be tied back to the spin rate ω_s through the following relations [10]:

$$\omega_p = -\left[\sin^2\theta_p + \left(\frac{I_1}{I_3}\cos\theta_p\right)^2\right]^{-\frac{1}{2}}\omega_s \tag{3}$$

$$\Omega_p = -\frac{I_3 - I_1}{I_3}\cos\theta_p\omega_p \tag{4}$$

And so, ϕ_p and ψ_p are linear functions of time, and the polhode angle θ_p is a constant governed by the kinetic energy of the spinning body.

In general, the polhode path is closed if there is no internal energy dissipation. However, internal energy dissipation, which can be caused by inelastic deformations, patch-effect-induced external currents, or magnetic hysteresis losses, will damp out the polhode motion, eventually aligning the $\boldsymbol{\omega}_s$ with I_3. Polhode motion can also be intentionally damped out by applying an external torque at the polhode frequency, using eddy currents, for example.

III. Test Mass Model

The MGRS test mass is a massive 50–100-mm-diam sphere. Although the choice of test mass material is an important issue for the MGRS design and its applications, this analysis only requires some assumptions about the TM shape, moments of inertia, and mass center offset from the geometric center. Therefore, we will not explicitly discuss materials.

The shape of a spherical TM is well described by expanding the sphere's radius in spherical harmonics:

$$r(\theta, \phi) = r_0 + \sum_{l=1}^{\infty}\sum_{m=-l}^{l} A_{lm}Y_{lm}(\theta, \phi) \tag{5}$$

The $l = 0$ term is removed from the summation and written explicitly as the nominal radius r_0. This expansion is performed in the body frame shown in Fig. 2a with spherical coordinates θ, ϕ measured with respect to the principal axes of inertia I_1, I_2, I_3, and origin at the TM mass center. We use the following definition of spherical harmonics and normalization constant:

$$Y_{lm}(\theta, \phi) = c_{lm}P_l^m(\cos\theta)e^{im\phi} \tag{6}$$

$$c_{lm} = \sqrt{\frac{2l+1}{4\pi}\frac{(l+m)!}{(l-m)!}} \tag{7}$$

Fabrication of spheres for the Gravity Probe B gyroscopes achieved shape irregularities ~20 nm peak-to-valley (~7 nm rms) [11]. In addition, measurements of the shape of these spheres fabricated by successive lapping and polishing indicate that the magnitude of the harmonics are typically inversely proportional to the harmonic number (i.e., $A_{lm} \propto l^{-1}$). This means that the magnitude of the shape irregularities are inversely proportional to their spatial size. Figure 3 shows the measured amplitude of the shape harmonics for one of the Gravity Probe B rotors plotted against harmonic number l. The amplitude of the lth harmonic is the rms of A_{lm} for $-l \leq m \leq l$. Therefore, one can think of Fig. 3 as the mean square spectral density of the TM shape irregularities, where l represents the spatial frequency for a sphere of unit circumference (number of undulations per revolution). The apparent l^{-1} trend corresponds to a constant maximum slope in the surface which is a plausible consequence on the lapping and polishing process.

The MC offset from the geometric center (GC) of the sphere is entirely captured by the A_{1m} terms in the expansion. The Gravity Probe B rotors, which were fabricated from fused quartz, had MC offsets ~10 nm, which was measured once in orbit [12]. However, density inhomogeneities for the materials proposed for the MGRS test mass could cause an MC offset ~1 μm if not properly controlled. Measurement of the MC offset of a spherical test mass has been made to ~300 nm, with the potential of achieving 100 nm in the near future [13]. If one can measure the MC offset to ~300 nm, then it is possible to reject test masses with MC offsets >300 nm, or to move the MC to within 300 nm of the GC in the fabrication process. It is on this basis that we assume a rough model for the sphere's shape defined by Eq. (5) with $A_{1m} \sim 300$ nm and $A_{l\neq 1m} \sim 30\ l^{-1}$ nm. This model for the TM shape is also plotted in Fig. 3 for comparison with a fabricated Gravity Probe B rotor. It is important to note that the measured harmonics plotted in Fig. 3 are relative to the geometric center of the sphere and not the mass center. Therefore, the contribution from the GC with respect to the MC is not included in the measured harmonics.

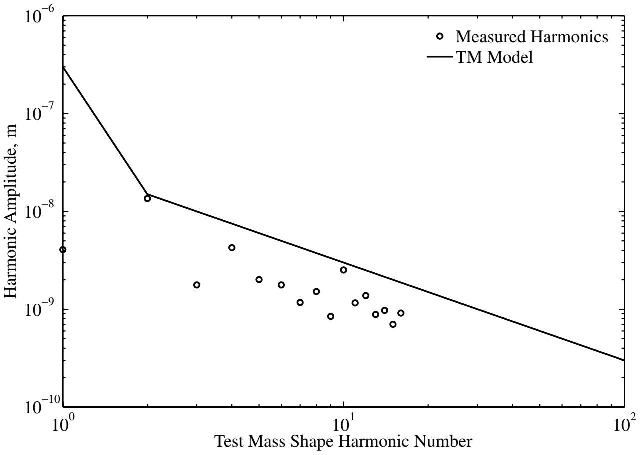

Fig. 3 Measured shape harmonics of a Gravity Probe B rotor and model for the MGRS test mass shape.

To have the polhode frequency above the science frequency band of 0.1 mHz–1 Hz, it is desirable to have the TM moment of inertia difference ratio $k_1 = (I_3 - I_2)/I_1 \geq 0.1$, so that, for a spin frequency $\omega_s/2\pi > 10$ Hz, the polhode frequency $\Omega_p/2\pi > 1$ Hz. This can be accomplished by using a TM with internally hollowed out portions and a spherical outer surface. To achieve a maximum average density so that the effect of surface forces are minimized, one would not like to see a reduction of average density of more than say 20%. There are a number of internal shapes for which $k_1 > 0.1$ and density loss is <20%. All of these geometries leave the third moment of inertia difference ratio $k_3 = (I_2 - I_1)/I_3 \sim 0$ so that the TM is nearly symmetric about the I_3 axis. As a consequence, the polhode phase ϕ_p and the precession phase ψ_p will both be linear functions of time, and the modulation of the science signal at precession and polhode frequencies will be purely sinusoidal.

Moments of inertia of test masses have been measured to 10^{-4} [14]. And so, it is possible to verify that $k_1 \sim 0.1$ and $k_3 \leq 10^{-4}$ before launch. This is enough to justify the assumption of a symmetric TM. For example, with $k_1 = 0.1$ and $k_3 = 10^{-3}$, and with $\boldsymbol{\omega}_s$ aligned within 0.5 rad of I_3, the time history of the orientation of the TM in the inertial frame only deviates by ~1 m rad from that of a purely symmetric body. Because any plausible optical sensor will have a spot size >1 m rad, orientation variations of this order are negligible.

IV. Model of Sensor Output

The combined output of the MGRS sensors must provide the test mass MC location measured relative to the geometric center of the spacecraft housing. We quantify the MC location with the vector **p** that defines the geometric center of the housing with respect to the test mass MC, because it is the MC that is inertially fixed. The measurement goal for the MGRS is 10 pm/$\sqrt{\text{Hz}}$ in the 0.1 mHz–1 Hz frequency band. Each sensor is assumed to be an optical sensor capable of measuring relative distances to ~3 pm/$\sqrt{\text{Hz}}$. A candidate sensor that meets this requirement with <10 μW of incident optical power is presented in [15].

Each MGRS sensor measures variations in the distance from a reference location on the housing to the surface of the test mass. The vectors $\mathbf{s}^k$ specify the locations of each of the $k = 1, 2, \ldots, K$ sensors relative to the geometric center of the housing, which is displaced from the TM mass center by $\mathbf{p}$. Instead of explicitly defining a third spacecraft reference frame where the sensor locations are defined, we can simply define $\mathbf{s}^k$ using inertial spherical coordinates (h^k, ξ^k, η^k) without loss of generality. The distance from the geometric center of the housing to sensor k is h^k, and ξ^k and η^k, which vary with changes in the spacecraft attitude, define the orientation of sensor k. Then, the location of sensor k in the inertial frame is $\mathbf{p} + \mathbf{s}^k$ (see Fig. 2b).

The magnitude of $\mathbf{p}$ is governed by the performance of the drag-free control system. We assume that $|\mathbf{p}| < 30\ \mathrm{nm}/\sqrt{\mathrm{Hz}}$ in the science measurement band, which is consistent with the LISA design requirements [2]. Therefore, we only need to work to first order in $\mathbf{p}$, because second- and higher-order terms will be below the measurement accuracy of $\sim 3\ \mathrm{pm}/\sqrt{\mathrm{Hz}}$. The output z^k of sensor k is the length of $\mathbf{p} + \mathbf{s}^k$ minus the sphere's radius in the direction to sensor k. Of second order is the effect of spacecraft motion perpendicular to the direction $\hat{\mathbf{s}}^k \equiv \mathbf{s}^k/|\mathbf{s}^k|$. Keeping only first-order terms in $\mathbf{p}$, we get the following for the sensor output:

$$z^k = h^k + \mathbf{p}\cdot\hat{\mathbf{s}}^k - r(\xi^k, \eta^k) \tag{8}$$

The expression for the sphere's radius [Eq. (5)] is fixed to the test mass, whose orientation is constantly changing with respect to the inertial frame where the sensor locations are defined. Using the Euler angles ϕ_p, θ_p, and ψ_p we can transform Eq. (5) from the body frame to the inertial frame. The resulting expression for spherical harmonics in the body frame in terms of spherical harmonics in the inertial frame is as follows:

$$Y_{lm}(\theta, \phi) = \sum_{n=-l}^{l} e^{in\psi_p} d^l_{mn}(\theta_p) e^{im\phi_p} Y_{ln}(\xi, \eta) \tag{9}$$

Here, $d^l_{nm}(\alpha)$ are rotation matrices commonly used in quantum mechanics. See [16] for details. Inserting this into the expression for the sphere's radius [Eq. (5)], we get an expression for the TM shape written in the inertial frame:

$$r(\eta, \xi) = r_0 + \sum_{l=1}^{\infty}\sum_{m=-l}^{l} A_{lm} \sum_{n=-l}^{l} e^{in\psi_p} d^l_{mn}(\theta_p) e^{im\phi_p} Y_{ln}(\xi, \eta) \tag{10}$$

Spinning the test mass at a high enough frequency, so that both the precession and polhode frequencies are above the frequency range of interest, allows us to separate the component of the sensor output due to the sphere's shape from the component containing the science signal. To explicitly illustrate this separation, we rearrange the sums in Eq. (10) to extract the components varying at the precession frequency $\omega_p/2\pi = \dot{\psi}_p/2\pi$ which is dominant. After inserting the resulting expression into Eq. (8), we get the following for the sensor output:

$$z^k = h^k + \mathbf{p}\cdot\hat{\mathbf{s}}^k - r_0 - \sum_{n=-\infty}^{\infty} H^k_n e^{in\psi_p} \tag{11}$$

$$H^k_n = \sum_{\substack{l=|n| \\ l\neq 0}}^{\infty}\sum_{m=-l}^{l} A_{lm} Y_{ln}(\xi^k, \eta^k) d^l_{mn}(\theta_p) e^{im\phi_p} \tag{12}$$

Equations (11) and (12) represent the full model for the MGRS sensor output including all contributions larger than the sensor accuracy of $\sim 3\ \mathrm{pm}/\sqrt{\mathrm{Hz}}$. Physically, H^k_n is the nth harmonic of the precession frequency measured by sensor k. If the polhode motion has not damped out, then all harmonics of this frequency including the zeroth are modulated at harmonics of the polhode frequency $\Omega_p/2\pi = \dot{\phi}_p/2\pi$. Because the optical spot is on the order of 0.1 mm and the TM diameter is $\sim$75 mm, averaging of the TM shape harmonics $l > \sim 1000$ occurs so that we only need to take the sum up to $\sim$1000. Effects of sensor nonlinearities are assumed to be perfectly accounted for.

V. Evaluation of Systematic Errors

We have derived an expression for the output of each MGRS sensor, Eq. (11), which is written in terms of harmonics H^k_n of the TM precession frequency. Later, we demonstrate that the precession frequency can be quickly and accurately determined from the sensor data. Knowing this frequency allows us to compute and subtract all harmonics from the sensor output, except for the $n = 0$ harmonic which also contains the science signal. What remains is

$$z^k_{n=0} = h^k + \mathbf{p}\cdot\hat{\mathbf{s}}^k - r_0 - \sum_{l=1}^{\infty}\sum_{m=-l}^{l} A_{lm} Y_{l0}(\xi^k, \eta^k) d^l_{m0}(\theta_p) e^{im\phi_p} \tag{13}$$

Notice that Eq. (13) still contains harmonics of the polhode frequency. If we assume that the polhode is not damped out, then the polhode frequency can be estimated using the same technique used to estimate the precession frequency. And so, we can once again perform a harmonic decomposition of Eq. (13), this time in terms of the polhode frequency, and compute and subtract all harmonics of polhode except for the $m = 0$ harmonic, which leaves

$$z^k_{\substack{n=0 \\ m=0}} = h^k + \mathbf{p}\cdot\hat{\mathbf{s}}^k - r_0 - \sum_{l=1}^{\infty} A_{l0} Y_{l0}(\xi^k, \eta^k) d^l_{00}(\theta_p) \tag{14}$$

Equation (14) can be written in a more transparent form using the definition of the spherical harmonics and the fact that $d^l_{00}(\theta_p)$ is simply a Legendre polynomial. Namely,

$$z^k_{\substack{n=0 \\ m=0}} = h^k + \mathbf{p}\cdot\hat{\mathbf{s}}^k - r_0 - \sum_{l=1}^{\infty} A_{l0} c_{l0} P_l(\cos\xi^k) P_l(\cos\theta_p) \tag{15}$$

Equation (15) represents what remains in the MGRS sensor output once precession and polhode frequencies are removed. These frequencies can be removed from the data without corrupting the science signal because both spin and polhode frequencies are design parameters that can be set above the science frequency band. From Eq. (15), we see that there are two types of systematic errors that can affect measurement of the TM mass center location $\mathbf{p}$ in the science frequency band: test mass and housing deformations captured by variations in parameters h^k, r_0, and A_{l0}, and orientation variations captured by ξ^k and θ_p.

A. Test Mass and Housing Deformations

The MGRS sensors measure the distance between the housing and the test mass surface. If we take the housing to be a spherical cavity with sensors located at coordinates (h^k, ξ^k, η^k), then housing deformations can be analyzed in terms of spherical harmonics. In this light, housing and TM deformations will contribute to the sensor output in the same way. The MGRS sensors are arranged in evenly distributed opposing pairs (see Fig. 1) over the surface of the housing. This design is chosen to balance radiation pressure on the TM and to make the MGRS insensitive to changes in the even harmonics of the TM and housing geometry during science operations.

The MGRS can be operated in two modes: a science mode and a calibration mode. In the science mode, the output of opposing pairs of sensors are essentially subtracted so that only odd-shaped harmonics are observable. Consequently, in the science mode, the first harmonic is the lowest-order geometric variation that can produce errors in the MC measurement. In the calibration mode, the output of opposing sensor pairs are summed so that only even-shaped harmonics are observable, whereas the MC motion becomes unobservable. While in this configuration, any changes in the even harmonics of the TM and housing shape can be checked and calibrated. We will mainly focus on the science mode because it is the primary mode of operation.

The largest source of geometric changes is due to thermal variations. A change in the uniform temperature of the MGRS would cause a uniform expansion of the TM or housing. Because the design is insensitive to changes in the zeroth harmonic of shape in the science mode, the requirements for the stability of the uniform temperature of the MGRS can be relatively liberal. However, a change in the temperature gradient across the MGRS in the direction of spin will cause a change in the A_{l0} harmonic of the TM and housing shape, which the MGRS is indeed sensitive to. Therefore, requirements need to be placed on the variations in the temperature gradient across the MGRS depending on the geometric size and material choice. The MGRS housing can be constructed from a material with low coefficient of thermal expansion to minimize the effect of thermal variations. The test mass is less sensitive to external thermal variations because of the vacuum gap between the housing and the surface of the TM. The housing is thermally coupled to the spacecraft through radiation and conduction. However, because the test mass is surrounded by a vacuum, it is only thermally coupled to the housing by radiation. Because radiative coupling is weak relative to conductive coupling, not only will the amplitude of the temperature variations in the TM be much less than that of the housing, but the characteristic time of these variations will also be orders of magnitude less than that of the housing.

B. Orientation Variations

From Eq. (15), we see that spacecraft attitude ξ^k and polhode angle θ_p variations can generate systematic errors in the science measurement if their contribution to the sensor output is larger than 10 $\text{pm}/\sqrt{\text{Hz}}$ in the science frequency band. These systematic errors exist because variations in the polar angle orientation of the TM relative to the spacecraft couple to the Y_{l0} harmonics of the sphere, which are symmetric about the I_3 axis and, consequently, do not get averaged out by the TM spin. Because both angular variations enter Eq. (15) in the same way, we can evaluate their impact simultaneously.

Using Eq. (15) and our TM model, Eq. (5), which accounts for both shape and MC offset, we can place a requirement on variations in the spacecraft attitude in the science frequency band. Because the polhode angle is strictly decreasing for a symmetric body due to internal energy dissipation, its variations are all at zero frequency. If we examine variations in the sensor output z^k due to variations in ξ^k, holding all other contributions fixed, we have

$$z^k(\xi^k) = \sum_{l=1}^{\infty} A_{l0} c_{l0} P_l(\cos\xi^k) \tag{16}$$

Using the TM model developed in Sec. III and shown in Fig. 3, which is based on the measured shape of a fabricated sphere, we take $A_{1m} \sim 300$ nm and $A_{l\neq 1m} \sim 30\ l^{-1}$ nm. By far, the largest contributor to variations in $z^k(\xi^k)$ is the MC offset which has a maximum rate of change at $\xi^k = \pi/2$. Therefore, we look at variations in $z^k(\xi^k)$ by taking the derivative of Eq. (16) with respect to ξ^k at $\xi^k = \pi/2$ and using properties of Legendre polynomials to get the following:

$$\left.\frac{\mathrm{d}z^k}{\mathrm{d}\xi^k}\right|_{\xi^k=\pi/2} = \sum_{l=1}^{\infty} A_{l0} c_{l0} l P_{l-1}(0) \tag{17}$$

To estimate the total contribution of all harmonics, take the root-sum-square of each term. As an order of magnitude approximation, if we assume that the laser spot size is ∼0.1 mm and the TM radius is ∼75 mm, then each sensor will average out all shape harmonics for which $l \geq \sim 1000$. Therefore, after summing up to $l = 1000$ and taking the root-sum-square, we get the following:

$$\left.\frac{\mathrm{d}z^k}{\mathrm{d}\xi^k}\right|_{\xi^k=\pi/2} \sim 300\ \text{nm/rad} \tag{18}$$

With this relation, we can place a rough bound of 30 $\mu\text{rad}/\sqrt{\text{Hz}}$ on spacecraft attitude variations in the 0.1 mHz–1 Hz band to limit the contribution of these effects to <10 pm with respect to TM mass center determination. This places a limit on the performance of the spacecraft attitude control system.

We can also use our model to a place limit on the maximum rate of change of ξ^k and θ_p at zero frequency. If these angles vary by more than the sensor spot size, they can couple to the high-order harmonics of the sphere's shape to generate a signal in the science band. We know that the maximum harmonic observable by the sensors is the $l \sim 1000$ harmonic. This harmonic has an angular size of $2\pi/1000 \sim 6$ m rad. Therefore, to generate a signal at 0.1 mHz, the low end of the science frequency band, the angular rate would be 0.6 μ rad/s. This places a limit on the maximum spacecraft angular rate and maximum polhode decay rate.

The 60 deg inclination of the LISA constellation causes spacecraft attitude variations at the annual frequency [2]. The maximum rate associated with this variation is roughly $(\pi/3)(2\pi)/(1\ \text{year}) \sim$ 0.2 μ rad/s, which is below our maximum limit.

In terms of the polhode decay rate, the best way to meet this requirement would be to either damp out the polhode or to wait for it to damp out naturally. The design of the MGRS test mass increases polhode damping, because internal energy loss is proportional to the square of the polhode frequency, which is relatively high (>1 Hz). There are several ways to actively or passively damp the polhode using magnetic fields. As an example, the Honeywell Electrically Supported Gyro used eddy-current damping to damp the polhode, so that optical detection of a "D" pattern on the pole could be acquired.

The design limits provided here for spacecraft attitude variations in the science frequency band and for maximum attitude and polhode decay rates are only meant to provide order of magnitude estimates. The true limits will depend on the actual TM size, shape irregularities, and MC offset, and the internal sensor used. In addition, the systematic errors due to TM and housing deformations and orientation variations discussed in this section represent only a small portion of the overall error budget for a science mission like LISA. A complete error budget for LISA is provided in [17], in which errors are categorized as either optical-path noise (important above a few millihertz) or TM acceleration noise (important below a few millihertz). The systematic errors discussed in this paper fall into the category of optical-path noise, for which the total error budget is 40 $\text{pm}/\sqrt{\text{Hz}}$ [2].

VI. Simplified Model

We have suggested that the polhode behavior be damped out to limit the effect of a changing polhode on the TM mass center determination. We now develop a simplified model of the MGRS sensor output where we assume that the polhode has damped out. The simplified model will accurately describe the MGRS sensor output when the polhode angle $\theta_p < 10\ \mu$ rad. We believe the simplification of working with a damped polhode is worth including this as a design feature of the MGRS.

Our general model can be used to analyze the specific case of a damped polhode by allowing $\theta_p \to 0$. In this case, the transformation from the body frame to the inertial frame only requires a single positive rotation about I_3 by angle $\phi_p + \psi_p$. Letting $\theta_p \to 0$ in Eqs. (3) and (4), we see that the total angular rate of the TM is $\Omega_p + \omega_p = -\omega_s$, as expected. The minus sign comes about because we define the spin vector $\boldsymbol{\omega}_s$ in the inertial frame, not in the body frame where Ω_p and ω_p are defined. Therefore, we only need one Euler angle $\phi_s = -(\phi_p + \psi_p)$ to describe the motion, which we call the spin phase. To perform the spherical harmonic rotation from the body frame to the inertial frame, we perform only a single rotation about the I_3 axis by the angle $-\phi_s$:

$$Y_{lm}(\theta, \phi) = e^{-im\phi_s} Y_{lm}(\xi, \eta) \tag{19}$$

Inserting this expression into Eq. (5) for the sphere's radius and with Eq. (8) for the definition of the sensor output, we arrive at the simplified model for the sensor output, expressed in terms of harmonics of the spin frequency $\omega_s/2\pi$:

$$z^k = h^k + \mathbf{p}\cdot\hat{\mathbf{s}}^k - r_0 - \sum_{n=-\infty}^{\infty} H_n^k e^{-in\phi_s} \tag{20}$$

$$H_n^k = \sum_{\substack{l=|n| \\ l\neq 0}}^{\infty} A_{ln} Y_{ln}(\xi^k, \eta^k) \tag{21}$$

VII. Processing the Sensor Output

Now that we have a model for the output of each MGRS sensor, we will describe one simple and robust method for processing the data to recover the TM mass center location to the required level. We will focus on the simplified model where it is assumed that the polhode is damped out and the spacecraft attitude is maintained to $<30\ \mu\,\mathrm{rad}/\sqrt{\mathrm{Hz}}$ in the science band. However, this approach can be modified to handle the case in which the polhode is not damped out, as long as the polhode decay rate does not exceed $0.6\ \mu\,\mathrm{rad/s}$.

The highest frequency of interest for the science measurement is 1 Hz. Assuming that the sensor output is sampled at a rate greater than 1 Hz, say 1 kHz, we can process short stretches of data, say 1 s in length, to provide an estimate of the TM mass center location to the required accuracy at 1 Hz. TM location information for drag-free control may be required at higher rates, but because the drag-free measurement requirement is more than a factor of 10^2 less accurate than that for science, simpler and perhaps more robust methods may be employed for the drag-free control. The following sections describe how these short term batches of sensor data can be processed to provide an estimate of the spin speed and MC location to the required accuracy of once every second.

A. Mass Center Determination

Looking at Eq. (20), the simplified model for the sensor output, we see that all of the fast time-varying components due to the TM shape and MC offset from the geometric center occur at multiples of the spin rate ω_s and can therefore be separated from the MC location $\mathbf{p}$. Simply using 1 s averaging to process the sensor output will not produce an MC measurement to <10 pm because the magnitude of the variations at spin harmonics are $\sim 10^4$ times larger and the spin period would never be exactly commensurate with the 1 s batch length. There are several possible methods of processing the sensor output, such as digital filtering or mapping of the surface irregularities, which require an independent determination of the spin frequency. Here, we present a fairly simple and robust method of processing the sensor output in real time, which is independent of spin frequency and TM orientation.

Assume for the moment that the TM spin frequency is known and that the spin phase ϕ_s over short periods (≤ 1 s) can be written as a linear function of time $\phi_s(t) = \omega_s(t - t_i)$, where t_i is the start time for batch i. Then, to process the individual sensor output, we perform a linear least-squares fit of the following model to the data:

$$z^k \approx z_0^k + \sum_{n=1}^{N} A_n^k \cos(n\phi_s) + B_n^k \sin(n\phi_s) \tag{22}$$

The A_n^k and B_n^k coefficients are equal to twice the real and negative imaginary parts of the complex harmonics of spin H_n^k defined in Eq. (21) for the simplified model. The number of harmonics N used in the fit does not need to be large because an analog filter would likely be used before digitization. What we are interested in is the zero frequency components z_0^k whose variations in the 0.1 mHz–1 Hz band predominantly contain the component of the MC motion $\mathbf{p}$ in the direction to sensor k. We can write this explicitly as

$$z_0^k \approx \mathbf{p}\cdot\hat{\mathbf{s}}^k + c^k \tag{23}$$

The quantity c^k is a bias in the measurement associated with the nominal TM to housing gap $h^k - r_0$ and the Y_{l0} harmonics of the TM shape. Because the MGRS sensors only measure distance variations, this bias is somewhat irrelevant. However, we keep it because it is the variations in this bias that can generate the systematic errors previously discussed. Note that $\mathbf{p}$ and $\hat{\mathbf{s}}^k$ can be written in any consistent reference frame. For example, we can choose to perform this dot product in a spacecraft fixed reference frame, so that $\hat{\mathbf{s}}^k$ are known fixed quantities and $\mathbf{p}$ provides a meaningful error signal for the drag-free control system.

To recover the MC location, we need to combine the zero frequency components of all of the MGRS sensors. Specifically, we form the matrix $\mathbf{S}$ containing the unit vectors $\hat{\mathbf{s}}^k$ defining the directions to each of the K sensors in the MGRS, as well as the vector $\mathbf{z}$ of zero frequency components measured by each sensor:

$$\mathbf{S} \equiv \begin{bmatrix} \hat{\mathbf{s}}^{1^T} \\ \hat{\mathbf{s}}^{2^T} \\ \vdots \\ \hat{\mathbf{s}}^{K^T} \end{bmatrix} \qquad \mathbf{z} \equiv \begin{bmatrix} z_0^1 \\ z_0^2 \\ \vdots \\ z_0^K \end{bmatrix} \tag{24}$$

We take the transpose of each unit vector, assuming that $\hat{\mathbf{s}}^k$ are all column vectors. Then, we can perform a least-squares fit to find the best estimate $\hat{\mathbf{p}}$ of the TM MC location:

$$\hat{\mathbf{p}} = \mathbf{S}^{\dagger}\mathbf{z} \tag{25}$$

We write the least-squares fit as a multiplication by the pseudoinverse $\mathbf{S}^{\dagger}$ because the location of each MGRS sensor is known and constant in a spacecraft fixed reference frame. Therefore, $\mathbf{S}^{\dagger}$ can be precomputed and stored onboard the spacecraft computer to simplify the real-time data processing.

B. Spin Frequency Determination

Fast and accurate algorithms for estimating the spin frequency of a spinning test mass onboard a drag-free spacecraft have been demonstrated [18]. In [18], trapped magnetic flux fixed to the surface of a superconducting test mass was measured using a dc SQUID magnetometer which is fixed to the spacecraft. We can apply similar techniques using the MGRS, whereby we measure irregularities in the TM shape, which are fixed to the surface of the TM, using interferometric displacement sensors which are fixed to the spacecraft.

Two techniques for spin frequency estimation are described in [18]: interpolation and phase differencing. The interpolation technique involves interpolating between the values of the peak bin and the two neighboring bins of a fast Fourier transform (FFT) of the measured signal. The exact spin frequency must lie between the peak frequency bin and one of its nearest neighbor bins. Using the analytical expression for the discrete Fourier transform of a simple sinusoid, one can appropriately weight the three largest bins in the FFT to produce a better estimate of the spin frequency than one would get by just using the peak bin frequency. The interpolation technique applied to actual flight data has been shown to provide a spin frequency estimate 1000 times more precise than an FFT alone [18].

Even greater precision has been achieved using the phase-differencing technique. Phase differencing involves comparing the phase of the FFT from two subsequent batches of short term data to refine an initial estimate of the spin frequency. The elapsed phase $\phi_2 - \phi_1$ between two times t_1 and t_2 is given by the following expression:

$$\phi_2 - \phi_1 = \omega_s(t_2 - t_1) - n2\pi \tag{26}$$

The integer number of spin cycles n between times t_1 and t_2 can be computed if the spin frequency is known to better than $1/(t_2 - t_1)$ Hz. Rearranging Eq. (26), we get the following estimate $\hat{\omega}_s$ of the spin speed:

$$\hat{\omega}_s = \frac{\phi_2 - \phi_1 + n2\pi}{t_2 - t_1} \tag{27}$$

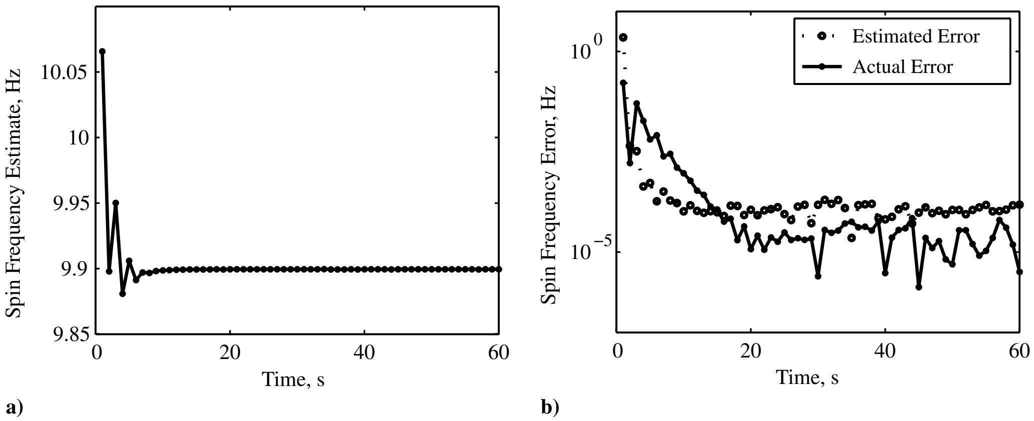

Fig. 4 Results from the combined algorithm: a) spin frequency estimate; b) estimated and actual spin frequency error.

Phase difference has been shown to provide a spin frequency estimate 10^5 times more accurate than an FFT alone [18].

C. Combined Algorithm

Test mass spin frequency and MC location determination algorithms can be combined in an elegant way to form a computationally tractable and robust method of processing the MGRS sensor data. Assume we evaluate consecutive 1 s batches of sensor data sampled at say 1 kHz. First, we need to generate an initial estimate of the spin frequency accurate to at least $1/2$ Hz. This can be done by either taking the first 1 s batch of data and applying the interpolation technique or by performing a simple FFT on several 1 s batches strung together. Once we have this initial estimate of the spin frequency $\hat{\omega}_s/2\pi$, we can apply the phase-differencing technique to continually refine the spin frequency estimate. Phase differencing and the spin harmonic fitting algorithm for MC estimation can be easily combined by noticing that the coefficients of the first harmonic of the spin frequency A_1^k and B_1^k can provide the necessary phase information for each 1 s batch. The following steps outline an iterative approach which combines the harmonic fits with the phase-differencing technique to continually estimate the TM mass center position and spin speed once per second.

1) Use $\hat{\omega}_s$ to perform a least-squares fit of the sensor data to spin harmonics, as in Eq. (22), to produce z_0^k for $k = 1, 2, \ldots, K$.
2) Combine all z_0^k to produce the best estimate of the TM mass center location $\hat{\mathbf{p}}$ using Eq. (25), and use this value for the science measurement and drag-free control system.
3) Estimate the TM spin phase at the start of the current batch using the first harmonic of spin measured by sensor k:

$$\phi_s^k(t_i) = \arctan\frac{-A_1^k}{B_1^k} \tag{28}$$

4) Compare the current spin phase $\phi_s^k(t_i)$ with the spin phase from the previous batch $\phi_s^k(t_{i-1})$ to generate a refined estimate of the spin frequency $\hat{\omega}_s$, accounting for the integer number of spin cycles between batches as in Eq. (27) and averaging over all K sensors.

Residual analysis and covariance techniques can be used to estimate the error in the MC determination, whereas the spin frequency error can be estimated by simply evaluating the standard deviation in the spin frequency estimates from each of the K sensors in the MGRS.

Numerical simulations accounting for realistic sensor noise and TM shape irregularities demonstrate that this technique is sensor noise limited and can reproduce the TM mass center motion to $<3\ \text{pm}/\sqrt{\text{Hz}}$ in the 0.1 mHz–1 Hz frequency band exceeding the $10\ \text{pm}/\sqrt{\text{Hz}}$ goal [19]. Using the output of only six sensors, the spin frequency estimation converges within 20 s to a relative error of $\sim 10^{-6}$, as shown in Fig. 4. The estimated spin frequency error also tracks the actual error to within one order of magnitude.

VIII. Conclusions

An analytical model for the modular gravitational reference sensor output, including all significant contributions, has been developed. This model is based on a spherical harmonic expansion of the test mass geometry which describes both surface shape irregularities and mass center offset from the geometric center. With a plausible description of the test mass geometry and moment of inertia tensor, test mass dynamics, including polhode motion, are also modeled using Euler's equations for torque-free motion. With this model, we conclude that the polhode should be damped out, which could be done as part of the initial spacecraft setup, and we can place limits on spacecraft attitude variations in the science frequency band and the maximum spacecraft angular rate.

A fast and reliable algorithm for recovering the mass center location and spin frequency of the test mass in real time has been presented. This iterative algorithm takes advantage of the sensor's high resolution, compared with the mass center offset, to track the spin phase and therefore the spin frequency. With the spin frequency, harmonics of spin present in the sensor output can be easily fitted and subtracted to recover the mass center variations that are of interest. The algorithm has been tested with simulated data, including realistic sensor noise and TM geometry, and has been shown to produce the mass center location and spin frequency to the required level of accuracy.

Acknowledgments

This work was supported by the ROSES Proposal Beyond Einstein Foundation Science 06-BEFS06-56, NASA Grant No. NNX07AK65G. The authors would like to acknowledge Mac Keiser, Sasha Buchman, Eric Gustafson, and Robert Byrer of Stanford for their prior work on optical detection of a spherical test mass for the Laser Interferometer Space Antenna mission. We would also like to thank Michael Salomon and Mike Dolphin of Gravity Probe B for their insights on rigid body dynamics and spin frequency estimation.

References

[1] Danzmann, K., and Rüdiger, A., "LISA Technology: Concept, Status, Prospects," *Classical and Quantum Gravity*, Vol. 20, May 2003, pp. S1–S9.
doi:10.1088/0264-9381/20/10/301

[2] LISA Study Team, "LISA, Laser Interferometer Space Antenna for the Detection and Observation of Gravitational Waves," Max-Plank-Inst. für Quantenoptik, Garching, Germany, LISA PrePhase A Rept. 233, July 1998.

[3] Jennrich, O. (ed.), Proceedings of the 5th International LISA Symposium and the 38th ESLAB Symposium, *Classical and Quantum Gravity*, Vol. 22, 2005.

[4] Phinney, E. S., "Big Bang Observer: Direct Detection of Gravitational Waves from the Birth of the Universe to the Present," NASA OSS Vision Missions Program, Proposal VM03-0021-0021, 2004.

[5] Sun, K.-X., Allen, G., Buchman, S., DeBra, D. B., and Byer, R. L., "Advanced Architecture for High Precision Space Laser Interferometers," *Classical and Quantum Gravity*, Vol. 22 No. 10, 2005, pp. S287–S296.
doi:10.1088/0264-9381/22/10/021

[6] DeBra, D. B., "Drag-Free Spacecraft as Platforms for Space Missions and Fundamental Physics," *Classical and Quantum Gravity*, Vol. 14, June 1997, pp. 1549–1555.
doi:10.1088/0264-9381/14/6/026

[7] Sun, K.-X., Allen, G., Buchman, S., Byer, R. L., Conklin, J. W., DeBra, D. B., Gill, D., Goh, A., Higuchi, S., Lu, P., Robertson, N., and Swank, A., "Modular Gravitational Reference Sensor for High Precision Astronomical Space Missions," *Bulletin of the American Astronomical Society*, Vol. 38 Dec. 2006, p. 991.

[8] Sun, K.-X., Allen, G., Buchman, S., Byer, R. L., Conklin, J. W., DeBra, D. B., Gill, D., Goh, A., Higuchi, S., Lu, P., Robertson, N. A., and Swank, A. J., "Progress in Developing the Modular Gravitational Reference Sensor," *AIP Conference Proceedings*, Vol. 873, No. 1, Nov. 2006, pp. 515–521.
doi:10.1063/1.2405093

[9] MacMillan, W. D., *Dynamics of Rigid Bodies (Theoretical Mechanics)*, 1st ed., Dover, New York, 1960, pp. 192–216.

[10] Greenwood, D. T., *Principles of Dynamics*, 2nd ed., Prentice–Hall, Upper Saddle River, NJ, 1988, pp. 408–421.

[11] Kahn, R., Everitt, C. W. F., Bencze, W., and Langentein, T., "Gravity Probe B Post-Flight Analysis Final Report," Stanford Univ., Technical Rept., March 2007.

[12] Dolphin, M., *Polhode Dynamics and Gyroscope Asymmetry Analysis on Gravity Probe B Using Gyroscope Position Data*, Ph.D. Thesis, Dept. of Aeronautics and Astronautics, Stanford Univ., Stanford, CA, 2007.

[13] Conklin, J. W., Sun, K.-X., and DeBra, D. B., "Mass Center Determination by Optical Sensing of Velocity Modulation," *AIP Conference Proceedings*, Vol. 873, Nov. 2006, pp. 566–570.
doi:10.1063/1.2405100

[14] Swank, A. J., Sun, K.-X., and DeBra, D., "Determining Gravitational Attraction by Mass Property Measurements," *AIP Conference Proceedings*, Vol. 873 Nov. 2006, pp. 588–592.
doi:10.1063/1.2405104

[15] Allen, G., Sun, K.-X., and Byer, R., "Using an Optical Fiber Fed Littrow Cavity as a Displacement Sensor for Use in Drag-Free Satellites," *AIP Conference Proceedings*, Vol. 873, Nov. 2006, pp. 334–338.
doi:10.1063/1.2405064

[16] Rose, M. E., *Elementary Theory of Angular Momentum*, Wiley, New York, 1957, pp. 48–57.

[17] Schumaker, B. L., "Disturbance Reduction Requirements for LISA," *Classical and Quantum Gravity*, Vol. 20, April 2003, pp. S239–S253.
doi:10.1088/0264-9381/20/10/327

[18] Salomon, M., *Properties of the Gravity Probe B Gyroscopes Obtained from High Frequency Squid Signal*, Ph.D. Thesis, Dept. of Aeronautics and Astronautics, Stanford Univ., Stanford, CA, 2008.

[19] Allen, G., Conklin, J. W., Sun, K.-X., DeBra, D. B., and Byer, R. L., "Mass Center Position Determination of a Spinning Sphere as Part of a Modular Gravitational Reference Sensor," Draft Paper, Stanford Univ., Stanford, CA, 2008, http://lisa.stanford.edu/lisawiki/StanfordDrafts.